THE JOURNAL OF BIOLOGICAL CHEMISTRY VOL. 281, NO. 3, pp. 1555–1563, January 20, 2006

ADAMTS13 Substrate Recognition of von Willebrand Factor A2 Domain*

Received for publication, July 29, 2005, and in revised form, September 22, 2005 Published, JBC Papers in Press, October 12, 2005, DOI 10.1074/jbc.M508316200

Sara Zanardelli, James T. B. Crawley[1], Chan K. N. Chan Kwo Chion, Jonathan K. Lam, Roger J. S. Preston, and David A. Lane

From the Department of Haematology, Imperial College London, London W12 ONN, United Kingdom

ADAMTS13 controls the multimeric size of circulating von Willebrand factor (VWF) by cleaving the Tyr[1605]–Met[1606] bond in the A2 domain. To examine substrate recognition, we expressed in bacteria and purified three A2 (VWF76-(1593–1668), VWF115-(1554–1668), VWFA2-(1473–1668)) and one A2-A3 (VWF115-A3-(1554–1874)) domain fragments. Using high pressure liquid chromatography analysis, the initial rates of VWF115 cleavage by ADAMTS13 at different substrate concentrations were determined, and from this the kinetic constants were derived (K_m 1.61 μM; k_{cat} 0.14 s^{-1}), from which the specificity constant k_{cat}/K_m was calculated, 8.70 × 10^4 M^{-1} s^{-1}. Similar values of the specificity constant were obtained for VWF76 and VWF115-A3. To identify residues important for recognition and proteolysis of VWF115, we introduced certain type 2A von Willebrand disease mutations by site-directed mutagenesis. Although most were cleaved normally, one (D1614G) was cleaved ~8-fold slower. Mutagenesis of additional charged residues predicted to be in close proximity to Asp[1614] on the surface of the A2 domain (R1583A, D1587A, D1614A, E1615A, K1617A, E1638A, E1640A) revealed up to 13-fold reduction in k_{cat}/K_m for D1587A, D1614A, E1615A, and K1617A mutants. When introduced into the intact VWFA2 domain, proteolysis of the D1587A, D1614A, and E1615A mutants was also slowed, particularly in the presence of urea. Surface plasmon resonance demonstrated appreciable reduction in binding affinity between ADAMTS13 and VWF115 mutants (K_D up to ~1.3 μM), compared with VWF115 (K_D 20 nM). These results demonstrate an important role for Asp[1614] and surrounding charged residues in the binding and cleavage of the VWFA2 domain by ADAMTS13.

Von Willebrand factor (VWF)[2] is a large multimeric plasma glycoprotein that mediates tethering and adhesion of circulating platelets at sites of vascular injury (1). Following endothelial damage, plasma VWF binds to the exposed sub-endothelial collagen (2). Once immobilized, the shear forces of the flowing blood induce a conformational transition that unravels the VWF molecule (3). This in turn exposes the binding sites for glycoprotein (Gp)Ibα, part of the GpIb-IX-V receptor on the surface of circulating platelets that confer platelet-tethering function (4). Once tethered, platelets become activated and subsequently present GpIIb/IIIa on their surface, which makes a tighter, more stable interaction with both VWF and fibrinogen. Activated platelets provide the phosphatidylserine-rich surface critical for the assembly of the procoagulant enzyme complexes that lead to the generation of thrombin (5).

VWF is expressed by endothelial cells and megakaryocytes (6). It is synthesized as 250-kDa monomers, which undergo intracellular processing-glycosylation, multimerization, and propeptide removal-that leads to formation of mature VWF multimers (7). Although much of endothelial VWF is constitutively secreted into the blood as multimers of varying size, a proportion is stored either within Weibel-Palade bodies in endothelial cells or within α-granules in platelets (8). These stored pools, which can be released upon specific stimulation, contain predominantly hyper-reactive "ultra-large" VWF that can exceed 2 × 10^4 kDa.

A wide range of VWF multimers (500–20,000 kDa) are found in normal plasma that differ only by the number of constituent VWF units. The largest VWF multimers unravel more readily in response to shear forces and contain more platelet binding sites. These species therefore confer the greatest hemostatic potential. The size of plasma VWF, and thus its platelet-tethering function, is regulated to prevent aberrant/spontaneous platelet-rich thrombus formation. VWF multimeric size is modulated by the plasma metalloproteinase ADAMTS13, which cleaves at a single site in the VWF A2 domain between Tyr[1605] and Met[1606] (9). This proteolysis can only proceed once VWF has been unraveled, either by rheological forces or *in vitro* in the presence of denaturants, both of which induce the exposure of the A2 domain scissile bond (10). Physiologically, this occurs upon VWF secretion from endothelial cells, limiting the thrombogenic potential of newly secreted ultra-large VWF by converting it into smaller multimeric forms (11). The nature of ADAMTS13 recognition of the A2 domain is poorly understood. In part, this is because of complex folding and interdependence of the A1-A2-A3 domains. This has been illustrated by proteolysis studies conducted with isolated domain fragments and certain VWF mutations that confer type 2A (group II) von Willebrand disease (VWD) (12–14). The latter are proximate or within the A2 domain and manifest enhanced ADAMTS13-dependent VWF proteolysis. This is thought to be because of structural changes that lead to constitutive/enhanced exposure of the A2 domain cleavage site (15).

Because of the uncertainty surrounding A2 domain recognition mechanisms by ADAMTS13, we have prepared both wild-type and variant A2 domain fragments that span the Tyr[1605]-Met[1606] cleavage site. For the first time, the cleavage of these by ADAMTS13 has been evaluated kinetically under normal physiological ionic conditions. We show that critical residues in the vicinity of the cleavage site are required for optimum cleavage and form part of an ADAMTS13 docking site within the A2 domain.

EXPERIMENTAL PROCEDURES

Expression and Purification of Recombinant ADAMTS13 and VWF Fragments—Recombinant human ADAMTS13 with a C-terminal Myc/His_6 tag was expressed and purified as previously described (16). For

* This work was supported by British Heart Foundation grants (to D. A. L. and J. T. B. C.). The costs of publication of this article were defrayed in part by the payment of page charges. This article must therefore be hereby marked "*advertisement*" in accordance with 18 U.S.C. Section 1734 solely to indicate this fact.

[1] To whom correspondence should be addressed: Dept. of Haematology, Faculty of Medicine, Imperial College London, 5th Floor, Commonwealth Bldg., Hammersmith Hospital Campus, Du Cane Rd., London W12 0NN, UK. Tel.: 44-20-8383-2297; Fax: 44-20-8383-2296; E-mail: j.crawley@imperial.ac.uk.

[2] The abbreviations used are: VWF, von Willebrand factor; HPLC, high pressure liquid chromatography; VWD, von Willebrand disease; Gp, glycoprotein; SPR, surface plasmon resonance; Tricine, *N*-[2-hydroxy-1,1-bis(hydroxymethyl)ethyl]glycine.

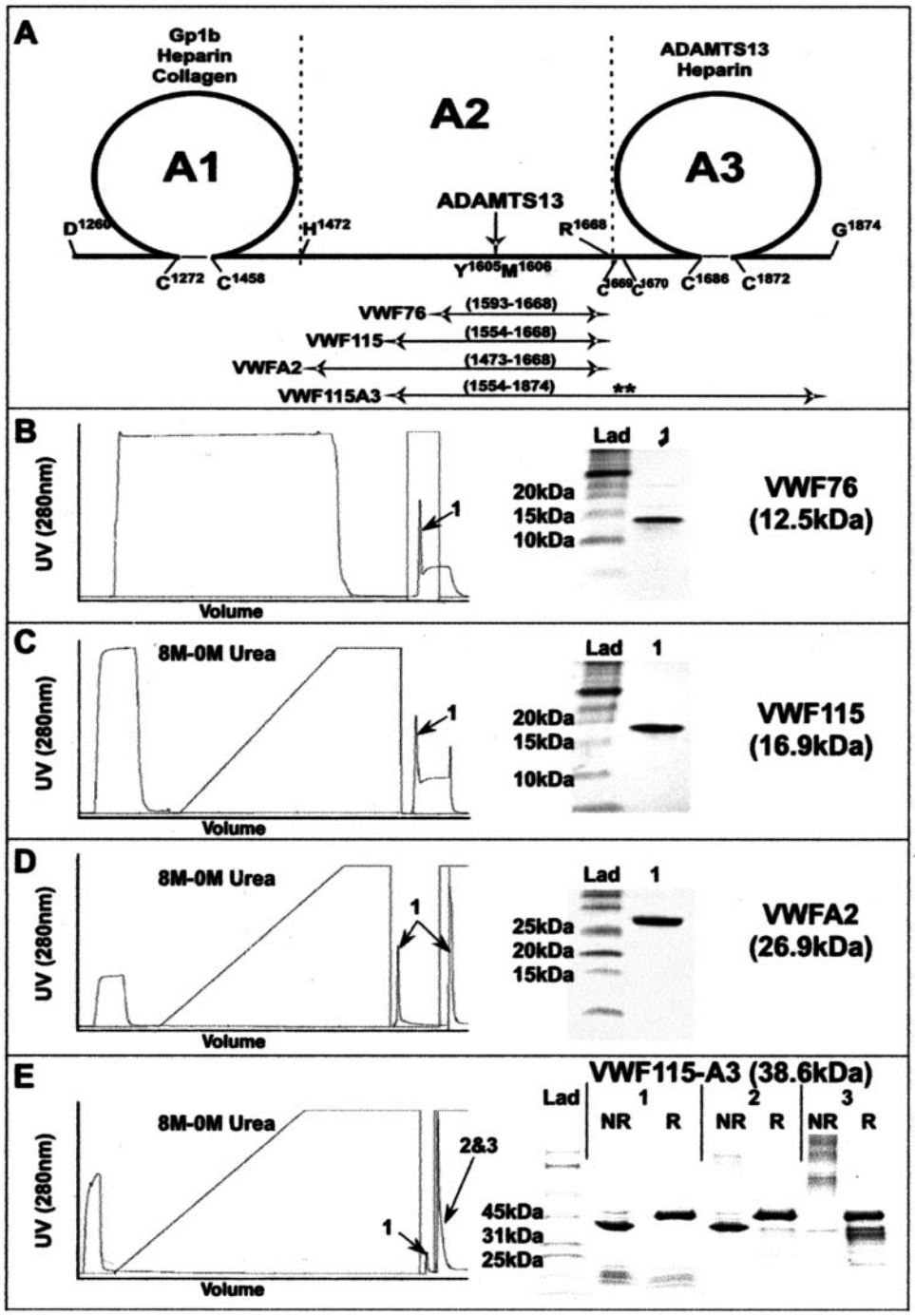

FIGURE 1. **Purification of recombinant VWF76, VWF115, VWFA2, and VWF115-A3.** *A*, diagram of the VWF A1A2A3 domains. A1 and A3 each contain paired cysteines, which are marked as are the amino acids at the boundary of each domain. Major ligands for each domain are highlighted. The ADAMTS13 cleavage site (Y^{1605}-M^{1606}) lies in the middle of the A2 domain. *Labeled arrows* represent the recombinant VWF fragments (*VWF76*, *VWF115*, *VWFA2*, and *VWF115-A3*) expressed in *E. coli*. All had an N-terminal polyhistidine/Xpress epitope tag. The VWF numbering of each substrate is given. In VWF115-A3, the 2 adjacent cysteine residues at 1669 and 1670 (**) were mutated to alanine. *B*, purification of VWF76 from cytoplasmic fraction extracted from transformed Rosetta *E. coli*. Chromatogram of VWF76 purification is shown. The eluted peak (*1*) was analyzed by SDS-PAGE and Coomassie staining. VWF76 was visualized as a single 12.5-kDa band, corresponding to its predicted mass. *C*, purification and refolding of VWF115 from inclusion body fraction extracted from transformed Rosetta *E. coli*. Inclusion bodies were solubilized with 8 M urea and refolded on a nickel-chelating column using an 8–0 M urea linear gradient. Chromatogram of VWF115 purification is shown. The eluted peak (*1*) was analyzed by SDS-PAGE and Coomassie staining. VWF115 migrated as a single 16.9-kDa band corresponding to its predicted mass. *D*, purification and refolding of VWFA2 from bacterial inclusion bodies. Inclusion bodies were solubilized with 8 M urea and refolded as for VWF115. Chromatogram of VWFA2 purification is shown. The eluted peak and stripped peaks (*1*) were dialysed and soluble material combined and analyzed by SDS-PAGE and Coomassie staining. As predicted, VWFA2 migrated as a 26.9-kDa band. *E*, purification and refolding of VWF115-A3 from Rosetta-Gami *E. coli* inclusion bodies. Insoluble material was solubilized and purified as for VWF115 and VWFA2. The eluted peak (*1*) and peaks stripped with 6 M guanidine/EDTA (2/3) were dialysed into 20 mM Tris (pH 7.8). The eluted peak (*1*), soluble stripped fraction (*2*), and insoluble precipitate after dialysis (*3*) were analyzed by reducing (*R*) and non-reducing (*NR*) SDS-PAGE and Coomassie staining. Under non-reducing conditions, soluble VWF115-A3 in *1* and *2* was visualized as a single 38.6-kDa band corresponding to its predicted mass. Correctly folded, monomeric VWF115-A3 was obtained within *fractions 1* and *2*. The presence of the disulfide bond was demonstrated by the band shift seen under reducing conditions. The insoluble precipitate contained predominantly VWF115-A3 polymers of higher molecular mass (*3-NR*).

surface plasmon resonance (SPR) and kinetic analysis experiments, an additional gel filtration step, using a Sephadex 26/10 column (Amersham Biosciences), was employed to obtain higher purity ADAMTS13.

The coding regions for different VWF A domain fragments (VWF76, Ser^{1593}-Arg^{1668}; VWF115, Glu^{1554}-Arg^{1668}; VWF115-A3, Glu^{1554}-Glu^{1874}; VWFA2, Met^{1473}-Arg^{1668}) were PCR amplified from the human VWF cDNA using *Pfx* high fidelity DNA polymerase (Invitrogen) according to the manufacturer's instructions. Fragments were cloned into the bacterial expression vector pET100/D-TOPO (Invitrogen), which fuses a His_6 and Xpress epitope tag to the N terminus of cloned sequences. As the VWF A3 domain contains two disulfide bonds, the adjacent paired cysteines at positions 1669 and 1670, at the start of the A3 domain, were mutated to alanine using the QuikChange XL kit (Stratagene). This approach improved yields of VWF115-A3 and ensured that the conserved A domain disulfide bond between Cys^{1686}-Cys^{1872} was correctly paired. Certain type 2A VWD mutations (R1597W, R1597Q, D1614G, I1628T, G1629R, E1638K) and specific charged residue substitutions (R1583A, D1587A, D1614A, E1615A, K1617A, E1638A, E1640A) were introduced into VWF115 and VWFA2 sequences using the QuikChange XL kit (Stratagene). All vectors were verified by sequencing.

VWF76, VWF115, and VWFA2 constructs were expressed in Rosetta *Escherichia coli* cells (Novagen, Nottingham, UK). VWF115-A3 was expressed in Rosetta-Gami *E. coli* (Novagen), which allows cytoplasmic disulfide bond formation. Transformed bacteria were grown in 2× yeast tryptone cultures at 37 °C with shaking. Once in log-phase growth,

recombinant protein expression was induced with 1 mM isopropyl-β-D-thiogalactoside for 16 h. Bacteria were harvested, and soluble (cytoplasmic) or insoluble (inclusion body) fractions were prepared using BugBuster reagent (Novagen). Recombinant His-tagged proteins were purified on an ÄKTA FPLC (Amersham Biosciences) using Ni^{2+}-HiTrap-chelating columns (Amersham Biosciences). VWF76 was purified from the soluble fraction according to the manufacturer's instructions and eluted with 500 mM imidazole. VWF115-A3, VWF115, and VWFA2 inclusion bodies were solubilized in 8 M urea/20 mM Tris-HCl (pH 7.8)/50 mM imidazole and bound to the Ni^{2+}-chelating column. Protein refolding was achieved using an 8–0 M urea linear gradient (1 ml/min for 40 min). Refolded, soluble material was eluted with 500 mM imidazole. Misfolded, precipitated protein was stripped from the column with 6 M guanidine/0.5 M EDTA. All recombinant proteins (eluted and stripped) were dialyzed into 20 mM Tris (pH 7.8) overnight at 4 °C. For VWFA2 and VWF115-A3, the stripped material was refolded by this process. Thereafter, soluble and insoluble protein fractions were separated by centrifugation. The purity of each recombinant protein was assessed by SDS-PAGE and Coomassie staining and quantified using a BCA total protein assay kit (Perbio, Cramlington, UK).

Cleavage of VWF Fragments by ADAMTS13—For time course reactions, recombinant ADAMTS13 (final reaction concentration 5–16.5 nM) was preincubated without substrate at 37 °C for 30 min in reaction buffer (final reaction concentrations 20 mM Tris, pH 7.8/150 mM NaCl/5 mM $CaCl_2$). In preliminary experiments, VWF76, VWF115, VWFA2, or VWF115-A3 were added as final concentrations of 4–8 μM to start each reaction. For analyses of the intact A2 domain, reactions were performed in the presence and absence of 1 M urea. At different time points, 65-μl sub-samples were removed and stopped with EDTA. 15 μl were analyzed by SDS-PAGE (16.5% Tris-Tricine gel; Invitrogen) and Coomassie staining. The remaining 50 μl were analyzed by HPLC. Samples were loaded on a BioBasic C4 column (Thermo Electron, Runcorn, UK), and the full-length and cleaved peptides were eluted/resolved using a specific acetonitrile gradient (20–55% for VWF76, 25–45% for VWF115, 25–60% for VWFA2, 20–65% for VWF115-A3). Mass spectrometry or N-terminal sequencing (Alta Bioscience, Edgbaston, UK) was performed to identify the polypeptide in each eluted peak and establish the precise site of proteolysis. For the determination of the specificity constant, low substrate concentrations $<K_m$ were used (250–500 nM substrate/5.5 nM ADAMTS13). Unicorn analysis software was used to calculate the areas under the peaks of the full-length and cleaved fragments. The measure of the catalytic efficiency, k_{cat}/K_m, was determined using Enzfitter software by fitting the data to Equation 1

$$k_{cat}/K_m = \frac{-\ln(1 - [AP]/[APf])}{et}$$

where $[AP]$ is the area under the cleavage product peak 1 curve at time t, $[APf]$ is the area under cleavage product peak 1 curve after complete cleavage, e is ADAMTS13 concentration, t is time. For individual determination of the K_m, V_{max}, and k_{cat}, the initial rate of proteolysis of VWF115 (after 5–10 min) was measured at varying substrate concentrations (100 nM-50 μM) as outlined above. Data were transformed into Michaelis-Menten and Lineweaver-Burk plots, and the catalytic constants were derived using Prism 4 software (GraphPad, San Diego, CA).

Surface Plasmon Resonance—SPR, using a dual flowcell BIAcore X biosensor system (BIAcore, Eyeworth, UK), was employed for analysis of the interaction between ADAMTS13 and different VWF115 variants. Two different SPR approaches were used. In each case, the surface of a carboxymethylated dextran (CM5) sensor chip (BIAcore) was activated with 0.4 M 1-ethyl-3-(3-dimethylaminopropyl)carbodiimide and 0.1 M *N*-hydroxysuccinimide, according to the manufacturer's instructions. First, ~600 response units of wild-type or variant VWF115 was covalently immobilized by amine coupling to one flow cell. To control for nonspecific binding, 600 response units of human endothelial protein C receptor was immobilized onto the other flow cell. All free reactive surface groups on both flow cells were blocked using 1 M ethanolamine. Different concentrations (10–137 nM) of ADAMTS13 in HBS-P buffer (BIAcore) were injected over both flow cells at 30 μl/min, contact time 1–2 min. After each injection, any bound ADAMTS13 was stripped with 10 mM NaOH prior to subsequent injections. Data analysis was performed using the BIAevalutaion software 3.0 (BIAcore), which allowed determination of k_a, k_d, and K_D values by fitting the derived sensograms to 1:1 Langmuir model. For the second approach, ~8000 response units of ADAMTS13 or anti-endothelial protein C receptor antibody (control) were immobilized to respective flow cells of CM5 chips, as above. Various concentrations (80 nM-1 μM) of VWF115, or VWF115 variants, in HBS-P buffer (BIAcore) were injected over both flow cells at 30 μl/min. The chip surface was regenerated with 10 mM NaOH as before. Using this approach, data were analyzed using a heterogeneous ligand (parallel reaction) model.

Modeling of VWF A2 Domain—The VWF A2 domain was computer modeled using its sequence homology to the VWF A3 domain and the coordinates for the crystal structure of this domain (Protein Data Bank code 1atz_A), according to the method outlined by Sutherland *et al.* (17). Models were manipulated using Protein Explorer (www.molvis.sdsc.edu/protexpl/frntdoor.html).

RESULTS

Purification of Recombinant VWF Fragments—Different human VWF A2 domain substrate fragments (Fig. 1*A*) were expressed in, and purified from, bacteria. VWF76 was purified from the soluble, cytoplasmic fraction by Ni^{2+}-chelating column affinity chromatography (Fig. 1*B*). SDS-PAGE and Coomassie staining demonstrated a purified product of 12.5 kDa. VWF115, VWFA2, and VWF115-A3 were purified from inclusion body preparations. Refolding of these proteins was achieved using an 8–0 M urea linear gradient during purification. This technique produced high yields of soluble VWF115 and VWFA2 of the correct predicted size (16.9 and 26.9 kDa, respectively) that were essentially pure (Fig. 1, *C* and *D*). VWF115-A3 was initially purified and refolded similarly. However, after elution a relatively low yield of soluble material was purified (Fig. 1*E*, *lane 1*). The precipitated protein was stripped from the column and refolded by dialysis, yielding higher amounts of soluble material (*lane 2*) than the on-column refolded preparation. The eluted material and the refolded/solubilized stripped fraction obtained after dialysis contained a product of 38.6 kDa (*lanes 1NR* and *2NR*). The presence of the disulfide bond between Cys^{1686} and Cys^{1872} was confirmed by the band shift upon reduction of this material (*lanes 1R* and *2R*). The insoluble material after dialysis contained VWF115-A3 polymers arising through intermolecular disulfide bond formation (*lane 3*) and was discarded.

Proteolysis of VWF76, VWF115, and VWF115-A3—To first visualize the capability of ADAMTS13 to proteolyze each of the recombinant A2 domain fragment substrates, recombinant ADAMTS13 was incubated at 37 °C with either VWF76, VWF115, or VWF115-A3 in the presence of physiological concentrations of Ca^{2+} and NaCl. Sub-samples were stopped between 0 and 6 h and analyzed by SDS-PAGE and Coomassie staining to give a qualitative assessment of each reaction (Fig. 2, *A–C*). In each case, only the full-length substrate band was visible at 0 h. Thereafter, the intensity of this band diminished and two smaller cleavage

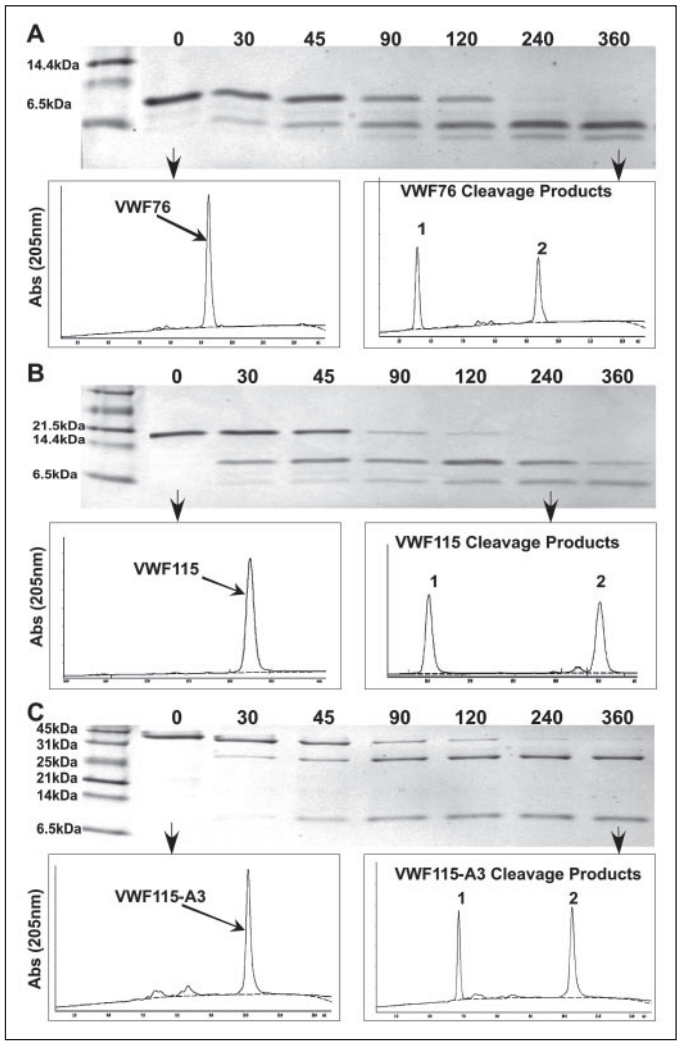

FIGURE 2. **Analysis of VWF76, VWF115, and VWF115-A3 proteolysis by ADAMTS13.** VWF76 (*A*), VWF115 (*B*), and VWF115-A3 (*C*) were incubated with ADAMTS13 as outlined under "Experimental Procedures." At various time points (0–6 h), sub-samples were stopped with EDTA and analyzed by SDS-PAGE/Coomassie staining and by HPLC, using a BioBasic C4 column. In each case (*A–C*), both techniques resolved the full-length substrate from the two cleavage products generated by ADAMTS13 proteolysis. Using the area under peak 1 as a measure of the extent of substrate proteolysis, this technique enabled quantification of the extent of proteolysis at each time point.

product bands appeared. In each case, these bands corresponded to the predicted molecular masses of fragments generated following cleavage at the Tyr^{1605}–Met^{1606} bond. N-terminal sequencing was performed upon the smallest cleavage product and confirmed that proteolysis had occurred between the Tyr^{1605}–Met^{1606} bond. Visually, VWF76, VWF115, and VWF115-A3 appeared to be proteolyzed by ADAMTS13 at similar rates. Parallel samples were also analyzed by HPLC. The resolution of the full-length substrate from the two cleavage fragments (*peaks 1* and *2*) arising from proteolysis (Fig. 2) of each different substrate allowed precise quantification of the extent of cleavage at each time point, confirming that the rates of proteolysis of VWF76, VWF115, and VWF115-A3 were, as indicated by the Coomassie staining, very similar (not shown).

To confirm specific proteolysis by ADAMTS13 and to identify each peak, cleavage product fractions were collected and analyzed by mass spectrometry. For all substrates, peak 1 corresponded to the tagged N-terminal cleavage product up to Tyr^{1605}. Peak 2 corresponded to the C-terminal fragment, in each case starting at Met^{1606}.

Type 2A VWD Mutations and ADAMTS13 Proteolysis—The scissile bond in VWF is predicted from a homology model (17) to be located in the center of the folded A2 domain (Fig. 3*A*). Given that VWF is the only known substrate for ADAMTS13 and that it is proteolyzed at just a single site, we hypothesized that other A2 domain amino acids that flank this site dictate the specificity of ADAMTS13 for the 1605–1606 bond. As an initial step toward identifying A2 domain residues that influence VWF proteolysis, we individually introduced six type 2A VWD mutations (see www.sheffield.ac.uk/vwf/) into the VWF115 construct (Fig. 3*A*). By mutating VWF115, which unlike the intact A2 domain naturally adopts a conformation that is permissive to ADAMTS13 proteolysis, the influence of specific mutations upon substrate specificity (as opposed to effects upon overall A2 domain structure) could be assessed under physiological ionic conditions. HPLC analysis of the proteolysis of VWF115 and VWF115 type 2A mutants (R1597W, R1597Q, D1614G, I1628T, G1629R, and E1638K) demonstrated that most of these mutations (R1597W, R1597Q, I1628T, and G1629R) had little or no effect upon VWF115 proteolysis (Fig. 3*B*). However, the E1638K mutant was proteolyzed slightly slower than VWF115, and the D1614G mutant was cleaved ~8 times slower (Fig. 3*B*). As Glu^{1638} and Asp^{1614} are charged residues that are predicted to be located in close proximity to each other on the surface of the VWF A2 domain homology model, we hypothesized that such residues might comprise part of an ADAMTS13 interaction site. Using this model, we subsequently identified additional acidic or basic amino acids predicted to lie on the surface of the A2 domain in the vicinity of Asp^{1614} and Glu^{1638} (Fig. 3*C*) and individually mutated each residue (Arg^{1583}, Asp^{1587}, Asp^{1614}, Glu^{1615}, Lys^{1617}, Glu^{1638}, Glu^{1640}) in VWF115 to alanine (Fig. 3*D*).

Kinetic Analysis of VWF76, VWF115, VWF115-A3, and VWF115 Charged Mutant Proteolysis—As a qualitative assessment of the relative ability of ADAMTS13 to proteolyze each of the charged residue mutants compared with the wild-type VWF76, VWF115, and VWF115-A3 substrates, we analyzed cleavage reactions by SDS-PAGE and Coomassie staining (Fig. 4*A*). From these gels, it seemed as if all of the mutants exhibited reduced rates of proteolysis. However, the concentrations of substrates needed to facilitate visualization by gel staining were high. To perform kinetic analysis of proteolysis for different substrates, it was necessary to monitor cleavage using substrate concentrations below the K_m for the reaction. Consequently, we determined the individual kinetic constants (K_m, k_{cat}) of VWF115 by measuring the initial rates of proteolysis at different concentrations (100 nM-50 μM). For the ADAMTS13-dependent proteolysis of VWF115 ($n = 4$), we derived a k_{cat} of 0.14 ± 0.06 s^{-1}. The K_m for this reaction was determined to be 1.61 ± 0.47 μM, from which a value for the specificity constant (catalytic efficiency, k_{cat}/K_m) of 8.70×10^4 M^{-1} s^{-1} could be derived.

For separate determination of the catalytic efficiency of VWF115, repeated time course experiments were performed using low substrate concentrations (250–500 nM). Repeated time course experiments ($n = 8$) gave a mean value of 7.83×10^4 M^{-1} s^{-1} for k_{cat}/K_m (Table 1). Confirmation of the pseudo-first order conditions was obtained by deriving the same k_{cat}/K_m value for VWF115 proteolysis at both 250 and 500 nM. Determination of k_{cat}/K_m for VWF76 and VWF115-A3 gave values of 6.39×10^4 M^{-1} s^{-1} and 6.70×10^4 M^{-1} s^{-1}, respectively (Table 1). These kinetic data confirmed that the VWFA3 domain does not significantly contribute to the rate of A2 domain proteolysis, despite containing an ADAMTS13 binding site (18).

The contribution of each selected charged amino acid to VWF proteolysis was assessed by determination of the catalytic efficiency of all the mutant VWF115 substrates at 500 nM (Fig. 4*C* and Table 1). The rate

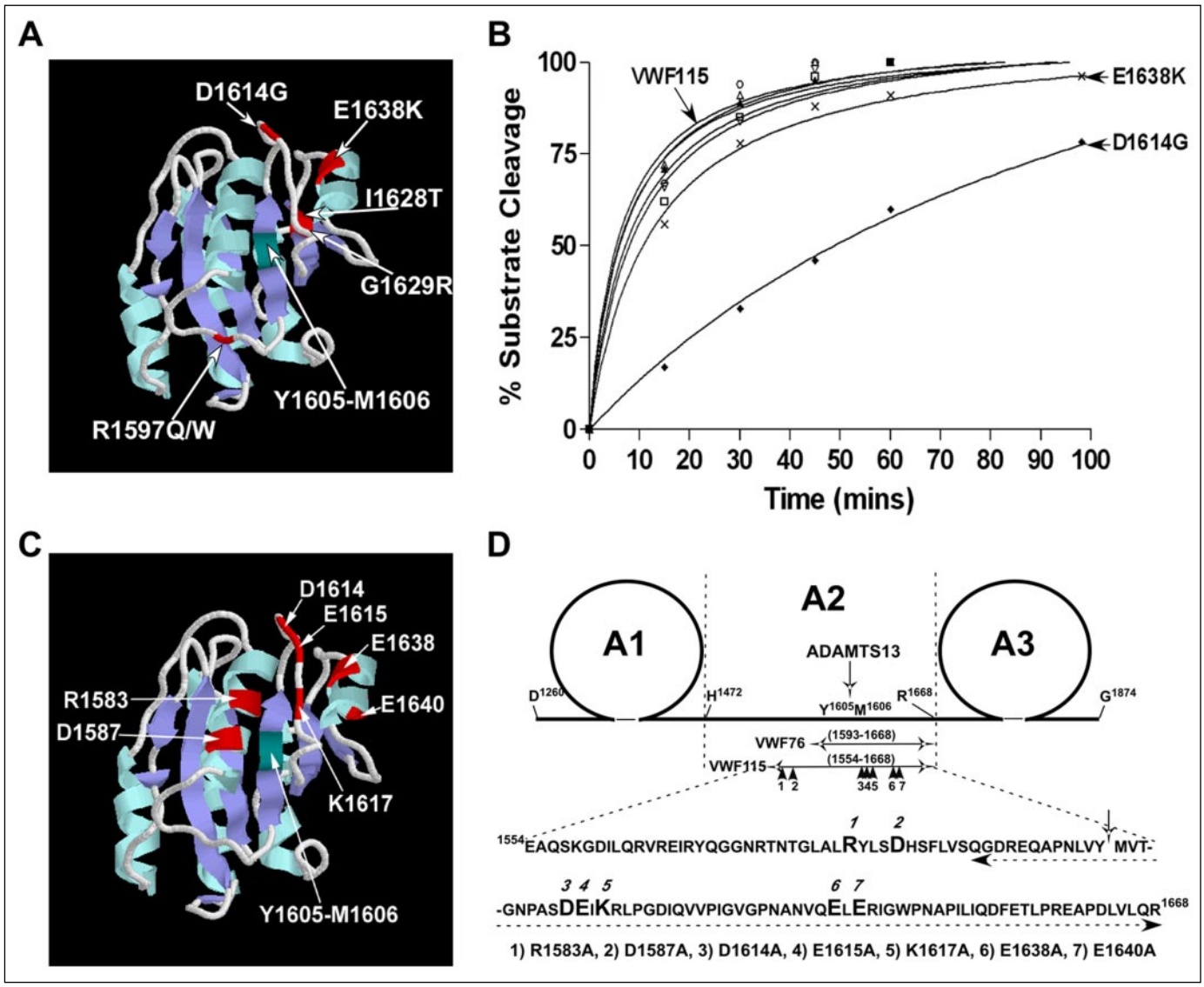

FIGURE 3. **Mutagenesis of VWF115.** *A*, predicted model of the VWF A2 domain. The Tyr[1605]–Met[1606] scissile bond in the center of the A2 domain is highlighted in *green*. The positions of certain type 2A (group II) VWD mutations that were introduced into VWF115 are labeled and highlighted in *red*. *B*, VWF115 and VWF115 type 2A mutants (R1597W, R1597Q, D1614G, I1628T, G1629R, E1638K) were proteolyzed with 10 nM ADAMTS13 and time course reactions analyzed by HPLC and represented graphically as in *panel B*). Although VWF115 and the R1597W, R1597Q, I1628T, and G1629R mutants were proteolyzed at very similar rates, the VWF115(E1638K) mutant was cleaved slightly slower. The VWF115(D1614G) mutant was proteolyzed at a markedly slower rate. *C*, predicted model of the VWF A2 domain. The Tyr[1605]–Met[1606] scissile bond in the center of the A2 domain is highlighted in *green*. The positions of the acidic/basic amino acids predicted to form a charged patch on the surface of the A2 domain in the vicinity of the most affected type 2A VWD mutants at Asp[1614] and Glu[1638] are highlighted in *red*. *D*, diagram of the VWF A1A2A3 domains. VWF76 and VWF115 regions are marked by *arrows*. The single letter amino acid sequence of VWF115 is given (VWF76 sequence is underlined with a *dashed arrow*). The ADAMTS13 cleavage site is marked (⇓). Locations of acidic and basic amino acids mutated to alanine and predicted to form a charged patch on the surface of the VWF A2 domain are highlighted (1–7).

of proteolysis of the R1583A mutant was not significantly different from that of VWF115, suggesting that this residue is not important for cleavage. Mutation of Glu[1638] and Glu[1640] induced a mild (2–3-fold) reduction in catalytic efficiency. The most affected (>12-fold reduction) single mutant was D1587A, the k_{cat}/K_m of which was $0.64 \pm 0.10 \times 10^4$ M^{-1} s^{-1}. The k_{cat}/K_m for K1617A, D1614A, and E1615A, which are predicted to lie on the same surface-exposed loop, were 1.90, 1.36, and 1.13×10^4 M^{-1} s^{-1}, respectively. These results implied that this loop might play an important role in the cleavage reaction. Consequently, we generated a triple mutant DEK1614/5/7AAA) containing all 3 residues substituted for alanine. Whereas individually these mutations caused a 4–7-fold reduction in k_{cat}/K_m, in combination the catalytic efficiency was >13-fold less than wild-type VWF115, implying that the amino acids in this charged loop may act in synergy.

Influence of D1587A, D1614A, and E1615A upon VWFA2 Proteolysis—To test whether the effects of the above mutations were maintained in a fully folded A2 domain, we introduced the most affected single charged mutants into the whole A2 domain. A variety of VWF A2 domain mutations appear to alter the conformation of the domain, such that the scissile bond is more readily exposed and thus more accessible for ADAMTS13 cleavage under normal physiological ionic conditions. Therefore, this approach also served to ascertain whether the most affected charged residue mutants (D1587A, D1614A, E1615A) induced gross structural changes. Despite using increased concentrations of ADAMTS13 (16.5 nM) in the absence of a denaturant, the intact wild-type A2 domain was proteolyzed very slowly, as visualized by gel staining (Fig. 5*A*), when compared with the A2 domain fragments VWF115, VWF76, and VWF115-A3. When samples containing 500 nM VWFA2

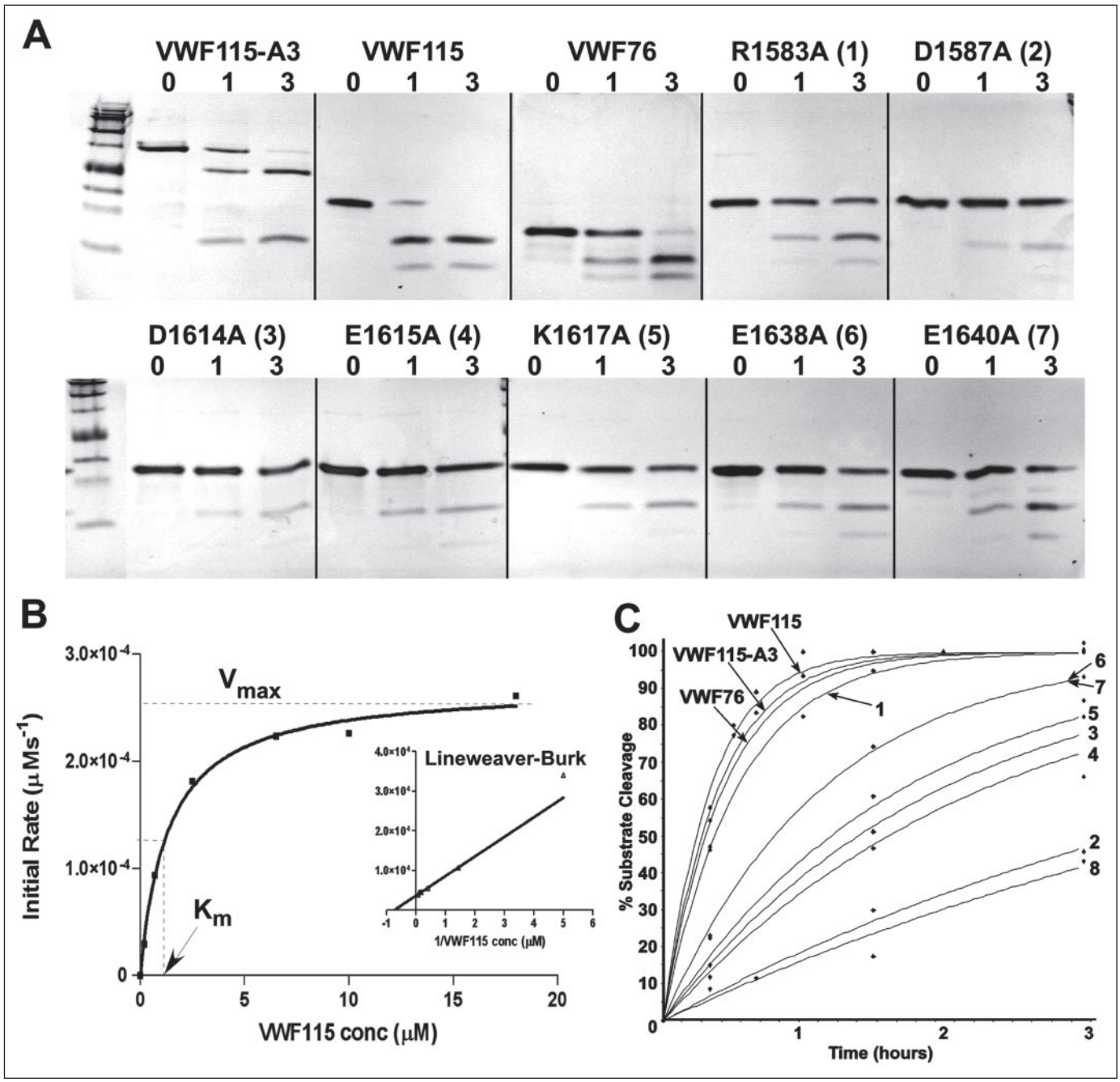

FIGURE 4. **Proteolysis of VWF76, VWF115, VWF115-A3, and VWF115 mutants by ADAMTS13.** *A*, SDS-PAGE and Coomassie staining of different substrate proteolysis. ADAMTS13 was incubated with different wild-type VWF A2 domain fragments or mutant VWF115 as indicated, using high substrate concentrations (4–8 μM). Samples analyzed were 0-, 1-, and 3-h time points. *B*, determination of the individual rate constants (K_m and k_{cat}) for VWF115 proteolysis by HPLC analysis of the initial rate of VWF115 proteolysis at different substrate concentrations (100 nM-50 μM). Michaelis-Menten and Lineweaver-Burk (*inset*) plots are shown. Values for K_m and k_{cat} for VWF115 proteolysis were 1.61 ± 0.47 μM and 0.14 ± 0.06 s^{-1}, respectively. *C*, HPLC analysis of time course reactions of different substrates shown in *panel A* are represented graphically. Reactions employed 500 nM substrate (marked as in *panel A*) and 8 nM ADAMTS13. The catalytic efficiency (k_{cat}/K_m) of proteolysis of each substrate was derived using Enzfitter software as shown in Table 1.

were analyzed by HPLC (Fig. 5*C*), it was clear that the cleavage reaction did not proceed toward completion (~28% after 5 h), as previously reported (13). The D1587A, D1614A, and E1615A VWFA2 mutants were proteolyzed either at a similar or slower rate (Fig. 5, *A* and *C*), suggesting that these mutations do not alter the A2 domain structure markedly. Under denaturing conditions (1 M urea), the wild-type VWFA2 was proteolyzed faster, although it still did not reach completion (~50% after 5 h) (Fig. 5, *B* and *D*). Although all the mutants were cleaved at a higher rate under denaturing conditions, they were cleaved appreciably slower than VWFA2, corroborating the direct influence of these mutations upon VWF115 proteolysis.

Confirmation of ADAMTS13 Binding Site Residues in VWFA2 Domain—We hypothesized that the most likely cause of the reduced catalytic efficiency of the affected VWF115 charged mutants was impaired binding to ADAMTS13. To measure the influence of each mutation upon the interaction of VWF115 with ADAMTS13, we performed SPR analysis. Monoclonal antibody-mediated orientation-specific coupling of either VWF115 or ADAMTS13 to the sensor chip was not possible due to the relatively fast off-rates of these molecules with the available antibodies to each ligand (not shown). Consequently, we covalently bound either VWF115 or ADAMTS13 to the sensor chip by amine coupling. With VWF115 bound to the chip and ADAMTS13

injected over the sensor, we monitored a concentration-dependent binding response indicative of a high affinity interaction (K_D, 20 nM) for this interaction (Fig. 6, *inset*). Determination of both the association and dissociation rates for the ADAMTS13-VWF115 interaction ($n = 3$) demonstrated a slow off-rate (1.72×10^{-3} s^{-1}), which would appear to be the major determinant for the high affinity binding. A second approach, in which ADAMTS13 was coupled to the sensor chip and varying concentrations of VWF115 injected, gave a similar high affinity binding component ($K_D \sim 15$ nM, not shown). These data demonstrate that the affinity of ADAMTS13 for VWF115 is significantly higher than is suggested by the K_m for VWF115 proteolysis.

SPR analysis of VWF115 mutants (D1587A, D1614A, E1615A, and DEK1614/5/7AAA) using both binding approaches revealed a markedly reduced affinity of ADAMTS13 for each of the mutants when compared with wild-type VWF115 (Fig. 6). Because of the low binding response measured, an accurate K_D could not be derived from the VWF115 mutant data. Despite the poor fitting the estimate for the K_D for the DEK1614/5/7AAA mutant was ~1.3 μM. It was clear that for each variant the binding with ADAMTS13 was appreciably compromised and thus the likely cause of their reduced specificity constants.

TABLE 1

Kinetic analysis of different VWF substrate proteolysis by ADAMTS13.

ADAMTS13 was incubated with 500 nM substrate under physiological ionic conditions at 37 °C. Sub-samples from each time course reaction were taken (0–6 h) and the extent of proteolysis measured by HPLC. The catalytic efficiency (k_{cat}/K_m) of proteolysis of each substrate was derived using Enzfitter software. The specificity constants for each VWF substrate/VWF115 variant is given (±S.E.). For VWF115, VWF115-A3, and VWF76, $n = 8$. For the least affected VWF115 variants (R1583A, D1640A, E1638A, and K1617) and the triple mutant DEK1614/5/7AAA, $n = 1$. For the most affected single mutants (D1614A, E1615E, and D1587), $n = 3$. Numbering as in Fig. 4.

VWF substrate	k_{cat}/K_m
	$\times 10^4$ M^{-1} s^{-1}
VWF115	7.83 ± 1.18
VWF115-A3	6.70 ± 2.78
VWF76	6.39 ± 1.18
R1583A (1)	6.19
D1640A (7)	2.74
E1638A (6)	2.74
K1617A (5)	1.90
D1614A (3)	1.36 ± 0.26
E1615 (4)	1.13 ± 0.30
D1587A (2)	0.64 ± 0.10
D1614A/E1615A/K1617A (8)	0.59

DISCUSSION

ADAMTS13 cleaves a single bond within the VWF A2 domain (9). Under static or low shear conditions, proteolysis is slow because of the globular conformation adopted by multimeric VWF. Moreover, the complex folding of the A2 and surrounding domains further conceals the scissile bond (10). The isolated intact A2 domain is also not readily proteolyzed by ADAMTS13 (19). In the absence of a denaturant, the intact domain (VWF residues Met^{1473}-Arg^{1668}) adopts a "non-permissive" structure that restricts access of ADAMTS13 (13). This is potentially explained by a VWF A2 domain model that suggests that the Tyr^{1605}–Met^{1606} bond lies buried within the center of the folded domain (17) and is thus not normally solvent exposed. However, incomplete VWF A2 domain fragments that span the ADAMTS13 cleavage site (*e.g.* VWF73 Asp^{1595}-Arg^{1668} and VWF115 Glu^{1554}-Arg^{1668}) have been shown, here and elsewhere (12, 20, 21), to be readily and specifically

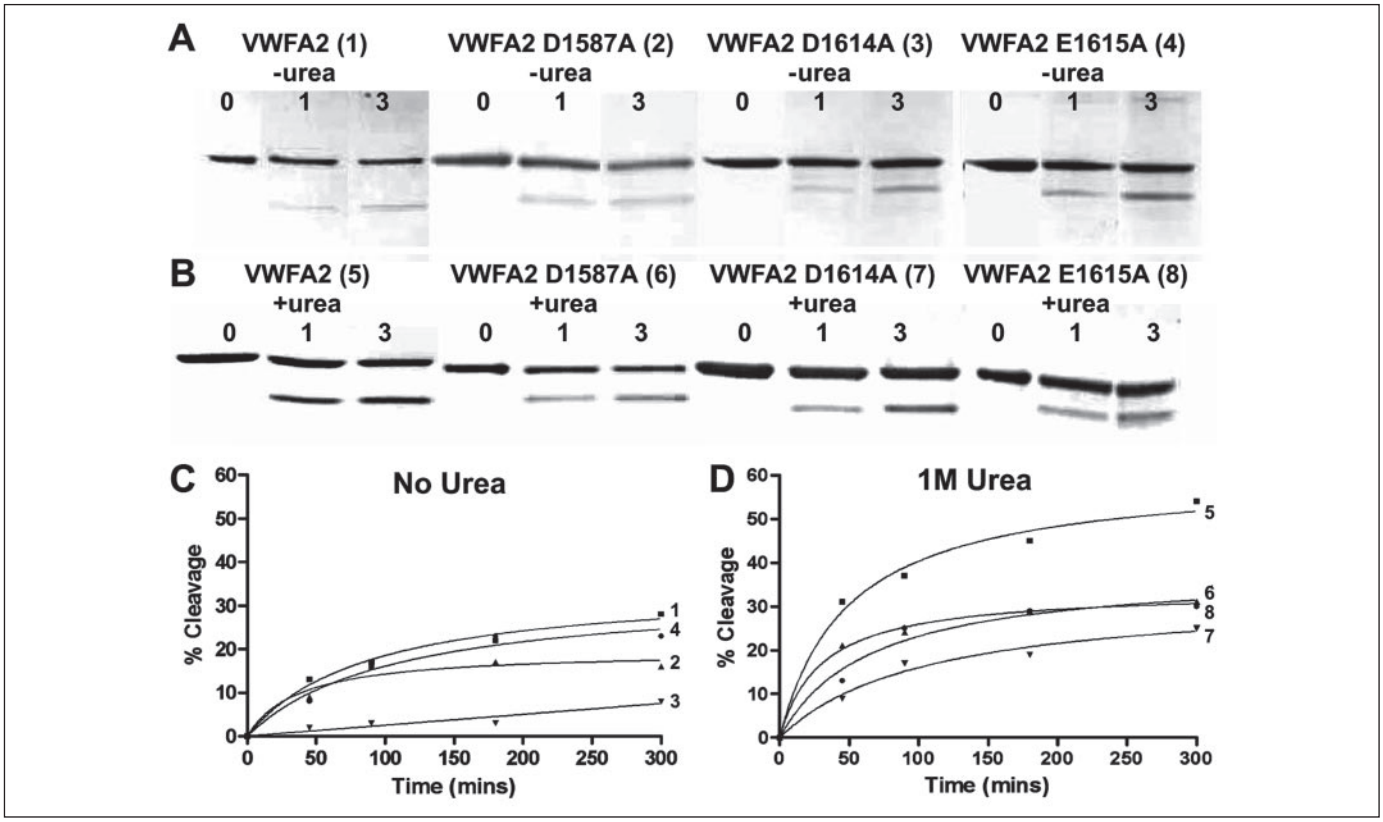

FIGURE 5. **VWFA2 and VWFA2 charged mutant proteolysis.** *A*, 6 μM VWFA2 (*1*) or VWFA2 carrying D1587A (*2*), D1614A (*3*), or E1615A (*4*) was incubated with 16.5 nM ADAMTS13 in the absence of denaturant and analyzed by SDS-PAGE and Coomassie staining. Samples were incubated for 0, 1, and 3 h as indicated. *B*, 6 μM VWFA2 (*5*) or VWFA2 carrying D1587A (*6*), D1614A (*7*), or E1615A (*8*) mutations was incubated with ADAMTS13 as in *panel A* in the presence of 1 M urea. Samples were analyzed as in *panel A*. *C*, graph of HPLC analysis of time course reaction samples 1–4 (*panel A*) set up in parallel reactions containing 500 nM of each substrate. *D*, graph of HPLC analysis of time course reaction samples 5–8 (*panel B*) set up in parallel reactions containing 500 nM of each substrate.

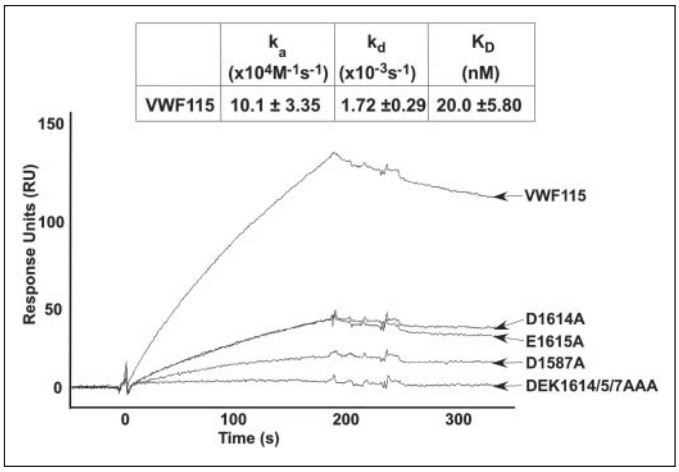

FIGURE 6. **Binding of ADAMTS13 to VWF115 and VWF115 mutants.** VWF115 was immobilized by covalently coupling 600 response units of VWF115 to one flow cell of a CM5 sensor chip and human endothelial protein C receptor to the control flow cell. Sequential injections of ADAMTS13 (10–137 nM) in HBS-P buffer were injected over the surface of each chip. Data were fitted using a 1:1 Langmuir model. Individual association (k_a) and dissociation (k_d) rates for the ADAMTS13-VWF115 interaction are given, from which the K_D (20.0 nM) was derived (k_d/k_a). Comparative SPR analysis was performed by covalently coupling VWF115, VWF115(D1587A), VWF115(D1614A), VWF115(E1615A) or VWF115(DEK1614/5/7AAA) as above. Results shown are overlaid data for VWF115 and VWF115(D1587A), VWF115(D1614A), VWF115(E1615A), or VWF115(DEK1614/5/7AAA) as marked, using 27.5 nM ADAMTS13.

cleaved at the Tyr^{1605}–Met^{1606} site under normal physiological ionic conditions, suggesting that these fragments not only contain important recognition sequences for specific ADAMTS13-dependent proteolysis but also that their structure presents the cleavage site in a permissive conformation, more akin to unraveled/denatured VWF (12). In the present study, we have expressed and purified a number of related VWF A2 and A2/A3 domain fragments to delineate those regions important for A2 domain proteolysis. Previous studies have employed SDS-PAGE and/or Western blotting to monitor proteolysis, the latter to achieve high sensitivity in the early stages of the cleavage reaction (13). Cleavage of VWF fragments by ADAMTS13 was quantified here by HPLC, allowing for the first time accurate and fully quantitative analysis of the kinetics of these reactions.

In our hands, most likely as a result of the smaller recombinant protein tag used in this study, VWF115 was marginally more susceptible to cleavage than the shorter substrate VWF76 (very similar to VWF73 that has been reported elsewhere (12, 20)) when the cleavage reaction was fully quantified. Its K_m was ~1.6 μM, $k_{cat} \sim 0.14\ s^{-1}$, and its specificity constant (k_{cat}/K_m) $\sim 8 \times 10^4\ M^{-1}\ s^{-1}$. This estimate of specificity is quite similar to that recently reported for ADAMTS13 cleavage of full-length VWF multimers under conditions of low ionic strength (22). This is surprising, considering those experiments were performed under denaturing conditions and without the advantage of a released peptide with which to accurately quantitate the rate of proteolysis. VWF115-A3 gave similar values for the specificity constant, suggesting that the A3 domain makes no appreciable contribution to the cleavage reaction despite its reported high affinity binding site (18). This finding corroborates previous semi-quantitative data obtained from the comparative analysis of recombinant VWFA2 and VWFA2/A3 proteolysis under denaturing conditions (13).

Residues surrounding the cleavage site are known to influence proteolysis of intact VWF, as they are reported to be dysfunctional in certain cases of type 2A (group II) VWD (15). We therefore introduced some of these mutations into the A2 domain fragment (VWF115) and evaluated proteolysis. Of course, the type 2A (group II) phenotype is generally associated with enhanced, rather than reduced, proteolysis by ADAMTS13. Nevertheless, we selected reported mutations surrounding the cleavage site, as not all had been tested extensively in terms of ADAMTS13 interaction. Interestingly, of those mutations selected, one (D1614G) was proteolyzed significantly slower when introduced into VWF115. To fully characterize how this mutation might exert a type 2A VWD phenotype, further studies examining its influence upon full-length, multimeric VWF will be required. Type 2A group II VWD mutations are generally believed to manifest their phenotype by unfolding of the A1-A2-A3 domain region, increasing ADAMTS13 access to, and therefore cleavage of, the scissile bond. The possibility of reduced, rather than enhanced, rates of cleavage of mutants, such as D1614G, in the vicinity of the cleavage site should be taken into consideration when evaluating the complex phenotype of cases of potential type 2A group II VWD. Because of this finding, we mutated further charged residues thought to be in proximity with Asp^{1614} on the basis of primary sequence and the homology model of the A2 domain. Of eight such mutants introduced into VWF115, six (D1587A, D1614A, E1615A, K1617A, E1638A, and E1640A) had clearly reduced cleavage rates. The triple mutant, DEK1614/5/7AAA, had ~13-fold reduction in the specificity constant for proteolysis. To confirm that the delayed cleavage of the VWF115 substrate was not merely a feature of this particular substrate, three of the mutations (D1587A, D1614A, and E1615A) were introduced into the fully folded intact A2 domain. Under denaturing conditions (1 M urea), proteolysis of all three substrates was reduced in rate and extent when compared with the wild-type VWFA2. Even under non-denaturing conditions, where under the conditions used proteolysis of the A2 domain did not exceed 30% at 300 min, proteolysis of D1587A and D1614A was appreciably impaired. These results with both VWF115 and A2 substrates suggested that specificity is appreciably influenced by a charged patch on the surface of the A2 domain.

Binding of ADAMTS13 to multimeric VWF and A2 domain fragment substrates has been reported to be of high affinity (23). Physiologically, ADAMTS13 seems to circulate in complex with VWF. However, the binding of ADAMTS13 to VWF need not necessarily be accompanied by proteolysis. Although Ca^{2+} ions are required for efficient proteolysis (10), they are not necessary for high affinity binding (21, 23). A recent report of binding of ADAMTS13 to VWF73 in the absence of Ca^{2+} ions using a microtiter plate-based immunoassay for ADAMTS13 suggested a K_D of 4.6 nM (21). Because of uncertainties surrounding the use of antibody detection and equilibrium perturbation in the detection step of binding in such assays, we used the alternative approach of SPR. Coupling VWF115 directly to the sensor chip and injecting different concentrations of ADAMTS13 yielded a K_D of ~20 nM. This high affinity interaction appeared to be conferred by a slow dissociation rate (k_d). Confirmation of tight binding was obtained by covalently immobilizing ADAMTS13 and then injecting VWF115 over the sensor chip. In this case, a K_D of 15 nM was obtained. However, there was also some evidence for heterogeneity of binding, and a lower affinity component was also apparent using this second approach. Importantly though, both SPR approaches demonstrated substantial loss (>10-fold) in binding affinity of ADAMTS13 to the mutant VWF115 fragments D1587A, D1614A, and E1615A and the triple mutant DEK1614/5/7AAA irrespective of whether SPR was performed with these fragments as analyte or ligand. This provides direct evidence that these residues form part of a docking site for ADAMTS13 on the VWFA2 domain.

The present investigation has for the first time identified critical residues within the VWF A2 domain that are important for both binding to ADAMTS13 and for proteolysis at the Tyr^{1605}–Met^{1606} bond. Given its specificity, proteolysis is unlikely to be determined solely by interaction with a limited number of residues surrounding the cleavage site. Previ-

ous studies have shown that although VWF73 is cleaved by ADAMTS13, a 9-residue deletion at the C terminus of this fragment completely abolished cleavage (12). It remains uncertain precisely where these 9 amino acids lie in the fully folded intact A2 domain or in unraveled multimeric VWF in relation to the charged patch/residues identified in this study. Despite this, and the inability of a peptide that spans this region to inhibit proteolysis, it remains possible that residues within this 9-amino acid sequence contribute directly to high affinity binding to the protease (12). Structures remote from the cleavage site are also known to influence proteolysis. The A1 domain of VWF was recently demonstrated to inhibit access of ADAMTS13 to the A2 domain cleavage site (13). This inhibition was removed in the presence of GpIbα, the principal A1 domain ligand, suggesting that under physiological conditions platelet binding may enhance VWF proteolysis either by increasing scissile bond access or by revealing an ADAMTS13 binding site.

Acknowledgment—We thank Dr. James Rance for help in the early phase of this work.

REFERENCES

1. Sadler, J. E. (1998) *Annu. Rev. Biochem.* **67,** 395–424
2. Roth, G. J., Titani, K., Hoyer, L. W., and Hickey, M. J. (1986) *Biochemistry* **25,** 8357–8361
3. Siedlecki, C. A., Lestini, B. J., Kottke-Marchant, K. K., Eppell, S. J., Wilson, D. L., and Marchant, R. E. (1996) *Blood* **88,** 2939–2950
4. Ruggeri, Z. M., De Marco, L., Gatti, L., Bader, R., and Montgomery, R. R. (1983) *J. Clin. Investig.* **72,** 1–12
5. Zwaal, R. F., Comfurius, P., and Bevers, E. M. (1998) *Biochim. Biophys. Acta* **1376,** 433–453
6. Bajaj, M. S., Kuppuswamy, M. N., Manepalli, A. N., and Bajaj, S. P. (1999) *Thromb. Haemostasis* **82,** 1047–1052
7. Haberichter, S. L., Fahs, S. A., and Montgomery, R. R. (2000) *Blood* **96,** 1808–1815
8. de Wit, T. R., and van Mourik, J. A. (2001) *Best Pract. Res. Clin. Haematol.* **14,** 241–255
9. Furlan, M., Robles, R., and Lammle, B. (1996) *Blood* **87,** 4223–4234
10. Tsai, H. M. (1996) *Blood* **87,** 4235–4244
11. Dong, J. F., Moake, J. L., Nolasco, L., Bernardo, A., Arceneaux, W., Shrimpton, C. N., Schade, A. J., McIntire, L. V., Fujikawa, K., and Lopez, J. A. (2002) *Blood* **100,** 4033–4039
12. Kokame, K., Matsumoto, M., Fujimura, Y., and Miyata, T. (2004) *Blood* **103,** 607–612
13. Nishio, K., Anderson, P. J., Zheng, X. L., and Sadler, J. E. (2004) *Proc. Natl. Acad. Sci. U. S. A.* **101,** 10578–10583
14. Tsai, H. M. (2004) *J. Thromb. Haemostasis* **2,** 2057
15. Tsai, H. M., Sussman, I. I., Ginsburg, D., Lankhof, H., Sixma, J. J., and Nagel, R. L. (1997) *Blood* **89,** 1954–1962
16. Crawley, J. T., Lam, J. K., Rance, J. B., Mollica, L. R., O'Donnell, J. S., and Lane, D. A. (2005) *Blood* **105,** 1085–1093
17. Sutherland, J. J., O'Brien, L. A., Lillicrap, D., and Weaver, D. F. (2004) *J. Mol. Model (Online)* **10,** 259–270
18. Dong, J. F., Moake, J. L., Bernardo, A., Fujikawa, K., Ball, C., Nolasco, L., Lopez, J. A., and Cruz, M. A. (2003) *J. Biol. Chem.* **278,** 29633–29639
19. Cruz, M. A., Whitelock, J., and Dong, J. F. (2003) *Thromb. Haemostasis* **90,** 1204–1209
20. Kokame, K., Nobe, Y., Kokubo, Y., Okayama, A., and Miyata, T. (2005) *Br. J. Haematol.* **129,** 93–100
21. Ai, J., Smith, P., Wang, S., Zhang, P., and Zheng, X. L. (2005) *J. Biol. Chem.* **280,** 29428–29434
22. De Cristofaro, R., Peyvandi, F., Palla, R., Lavoretano, S., Lombardi, R., Merati, G., Romitelli, F., Di Stasio, E., and Mannucci, P. M. (2005) *J. Biol. Chem.* **280,** 23295–23302
23. Majerus, E. M., Anderson, P. J., and Sadler, J. E. (2005) *J. Biol. Chem.* **280,** 21773–21778